



### **Science Arts & Métiers (SAM)**

is an open access repository that collects the work of Arts et Métiers Institute of Technology researchers and makes it freely available over the web where possible.

This is an author-deposited version published in: <https://sam.ensam.eu>  
Handle ID: <http://hdl.handle.net/10985/24787>

#### **To cite this version :**

Paul FRANCOIS, Jacques Andre ASTOLFI, Xavier AMANDOLESE - Experimental analysis of trailing edge hydroelastic coupling on a hydrofoil - Journal of Fluids and Structures - Vol. 125, p.104078 - 2024

Any correspondence concerning this service should be sent to the repository

Administrator : [scienceouverte@ensam.eu](mailto:scienceouverte@ensam.eu)



# Highlights

## **Experimental analysis of trailing edge hydroelastic coupling on a hydrofoil**

P. François, J.A. Astolfi, X. Amandolese

- Experimental evidence of hydroelastic trailing edge vibrations on a hydrofoil model at critical Reynolds numbers
- Highlight of the effect of moderate angles of attack on the trailing edge vibrations
- Highlight of the fluid-structure mechanism involved : the trailing edge hydroelastic coupling in the bounded frequency of amplification of Tollmien–Schlichting waves.
- Validation of a passive mitigating solution with negligible impact on the hydrofoil hydrodynamics performances
- New PIV post processing to map the boundary layer transition area

# Experimental analysis of trailing edge hydroelastic coupling on a hydrofoil

P. François<sup>a</sup>, J.A. Astolfi<sup>a</sup>, X. Amandolese<sup>b</sup>

<sup>a</sup>*French Naval Academy Research Institute, IREnav EA 3634, Brest, France*

<sup>b</sup>*LMSSC, Conservatoire National des Arts et Métiers, Paris, France*

---

## Abstract

This paper explores the conditions for hydroelastic trailing edge vibrations generating tonal noise on a NACA0015 aluminium hydrofoil clamped in a hydrodynamic tunnel. Tests were performed for Reynolds numbers  $Re$ , ranging from  $2 \times 10^5$  up to  $12 \times 10^5$  and various angles of attack  $\alpha$ , from 0 up to  $10^\circ$ . A laser vibrometer was used to characterize the hydrofoil vibratory response. Time Resolved Particle Image Velocimetry (TR-PIV) was used to scrutinize the origin of the hydrodynamic excitation mechanism. Hydroelastic trailing edge vibrations of significant amplitude were observed at moderate angles of attack  $4 \leq \alpha \leq 8.5^\circ$ , for Reynolds number such that the pressure side boundary layer transition was located close to the trailing edge, with a frequency signature allowing a lock-in with the hydrofoil trailing edge structural mode. Two passive solutions were tested to mitigate this hydroelastic flow-induced vibration : a truncated hydrofoil and a triggered one. The truncated configuration slightly impacts the vibration while triggering the pressure side boundary layer transition ahead of the trailing edge eliminates the trailing edge vibrations with negligible impact on the hydrofoil hydrodynamics

---

\*. Corresponding author

*Email address:* paul.francois@ecole-navale.fr (P. François)

performances.

*Keywords:* Hydrofoil, Hydroelasticity, Trailing-edge vibration, Experimental analysis, Boundary layer transition

---

## 1. Introduction

As it can affect performances, prone structural failures, disturb users, impact acoustic discretion and the whole surrounding ecosystem, noise and vibrations of hydrodynamic lifting surfaces are a matter of great concern. According to Blake *et al.* (1984) three unsteady flow mechanisms can be responsible for the vibration of a hydrofoil operating at low angles of attack. The first one is due to the unsteadiness of the incoming flow generating unsteady random hydrodynamic loading and a so-called buffeting response of the hydrofoil. The second one can also be classified as turbulence-induced vibration as it is the consequence of the unsteady random hydrodynamic loading due to the turbulent boundary layer on the hydrofoil surface. It thus mainly concerns hydrofoil operating at high Reynolds numbers. The third one is due to a tonal flow excitation generated by a periodic vortex shedding from the trailing edge. For hydrofoils with a blunt trailing-edge the vortex wake organisation can be regarded as a Kármán vortex street (Toebes, 1961). But for hydrofoils with a sharp trailing-edge, the exact mechanism that can be responsible for a discrete frequency organisation of the wake remains unclear. In that context, works conducted on airfoil tonal noise in the last decades are of great interest. The first mention of discrete frequency tones from a sharp-trailing-edge airfoil at moderate Reynolds number is probably from Clark (1971). Paterson *et al.* (1973) also mentioned tonal noise on an airfoil at moderate angle of attack  $\alpha = 6^\circ$ , for a Reynolds number close to  $8 \times 10^5$ . They introduced a frequency evolution law based on a constant Strouhal number  $St = 0.1$ , the Strouhal number being defined as  $St = 2f\delta/U_\infty$  where  $f$  is the frequency tone,  $U_\infty$  the mean flow speed and  $\delta$  the boundary layer thickness at the trailing edge (for either the suction or pressure side). Using the Blasius solution for a flat plate with no pressure gradient, the

frequency evolution law reads (Paterson *et al.* , 1973) :

$$f = \frac{0.011U_{\infty}^{1.5}}{\sqrt{c\nu}}, \quad (1)$$

where  $c$  is the chord of the hydrofoil and  $\nu$  the fluid kinetic viscosity.

Tam (1974) questioned this simple Strouhal number correlation and the Kármán vortex type organisation of the wake. He suggested that the tones are generated by a self-excited feedback loop involving unstable disturbances in both the boundary layer and near wake flow, along with the feedback of acoustic waves. Using this feedback loop model, a ladder type evolution of the dominant frequency, based on Shen (1954) and Lin (1945) stability curves, can be drawn and it crosses the Strouhal law of Paterson *et al.* (1973). Following the work of Tam (1974), Arbey (1983) assumed that the ladder-type evolution of the frequency can be due to an aeroacoustic feedback loop involving the diffraction of Tollmien-Schlichting (T-S) instabilities by the trailing edge. In an attempt to clarify the tonal noise generation mechanism on aerofoils at moderate Reynolds numbers, Nash *et al.* (1999) conducted experiments on a NACA0012 aerofoil section at  $6^\circ$  of incidence. They showed that the ladder type evolution of tones could be eliminated in anechoic wind tunnel conditions. Their results also revealed the presence of strongly amplified boundary-layer instabilities just upstream of the pressure surface trailing edge, rolling up to form a regular Kármán-type vortex street. They proposed a new mechanism for tonal noise generation based on the growth of T-S instability waves amplified by inflectional profiles close to the trailing edge pressure surface. In another paper, McAlpine *et al.* (1999) focused their work on the stability of the pressure side boundary layer in a way to understand the relationship between T-S waves and tonal noise. They conducted experiments on two aerofoils, including

an asymmetrical one, in order to highlight the impact of airfoil shape on the tonal frequency noise. They also mentioned that tonal noise is closely dependent on the presence of a Laminar Separation Bubble (LSB) on the pressure side close to the trailing edge. Nakano *et al.* (2007) carried out experiments to clarify the impact of the angle of attack on the tonal noise mechanism at moderate Reynolds number  $Re = 1.6 \times 10^5$ . Using liquid-crystal visualization and Particle Image Velocimetry, they confirmed that the tonal noise appearance at a low angle of attack is strongly linked to the location of the reattachment point of a LSB near the trailing edge on the pressure side.

More recently, Probsting *et al.* (2015) focused on a NACA0012 airfoil emitting tonal noise. They found that for an angle of attack of  $1.2^\circ$  and for  $Re \leq 4.5 \times 10^5$ , tonal noise emission could also be due to an acoustic feedback involving an LSB formed on the suction side of the airfoil.

In water, discrete frequency excitation mechanism involving an LSB on the suction side of a hydrofoil was also observed by Ducoin *et al.* (2012). Based on experiments conducted on a NACA66312 laminar hydrofoil at low angles of attack and transitional Reynolds numbers, they showed that the frequency of the boundary-layer transition mechanism can lock-in with some natural frequencies of the hydrofoil, leading to significant vibrations. Unsteady flow signature, downstream of the suction side LSB of a NACA66 hydrofoil was also investigated by Ducoin *et al.* (2019). Using DNS simulation along with experimental wall pressure measurements, they highlighted a coherent vortex shedding organisation downstream the LSB, for which the frequency evolution with the velocity matches the one of the Paterson law (1). They also confirmed that this vortex organisation further degenerates in turbulence after the breaking of T-S waves.

Following those works, the first aim of the current study is to clarify the angle of attack configurations leading to strong hydroelastic coupling close to the trailing edge on a symmetric NACA0015 hydrofoil operating at moderate Reynolds numbers. The second aim is to experimentally validate a simple passive solution to suppress those trailing edge vibrations and associated tonal noise.

The experimental set-up along with the hydrofoils modal characteristics are presented in Section 2. Results and discussions focusing on the trailing edge vibrations, wake organisation and mitigating solutions are reported in Sections 3 and 4, prior to a conclusion.

## 2. Materials and methods

Experiments were performed in the hydrodynamic tunnel of the French Naval Academy Research Institute (IRENav) in a square test section of  $0.192m \times 0.192m$  having a honeycomb standardized inlet flow (Figure 1). An aluminium NACA0015 section model hydrofoil of Young modulus  $E = 69\text{GPa}$ , a constant chord  $c = 0.1m$ , a maximum thickness of  $0.015m$  and a span  $s = 0.191m$  was clamped in a dedicated mounting system allowing the measurement of the lift, drag and pitching moment, thanks to a load cell sensor (see Figure 2). Note that due to the intrinsic flexibility of the SIXAXES® load cell system this is not an ideal clamped-free configuration and this will be discussed regarding the hydrofoil eigenmodes in section 2.2. Tests were performed for flow speed regulated from 2 up to  $12\text{ m s}^{-1}$  (i.e. a Reynolds numbers range, referred to the chord, from  $2 \times 10^5$  up to  $12 \times 10^5$ ). The longitudinal (referred to the  $x$  direction, see. Fig. 1) and vertical (referred to the  $y$  direction) turbulence intensities, measured in the test section without the hydrofoil model, vary in this flow velocity range from 1.5% up to 1.9% (longitudinal turbulence



intensity) and from 0.8% up to 1.25% (vertical turbulence intensity).

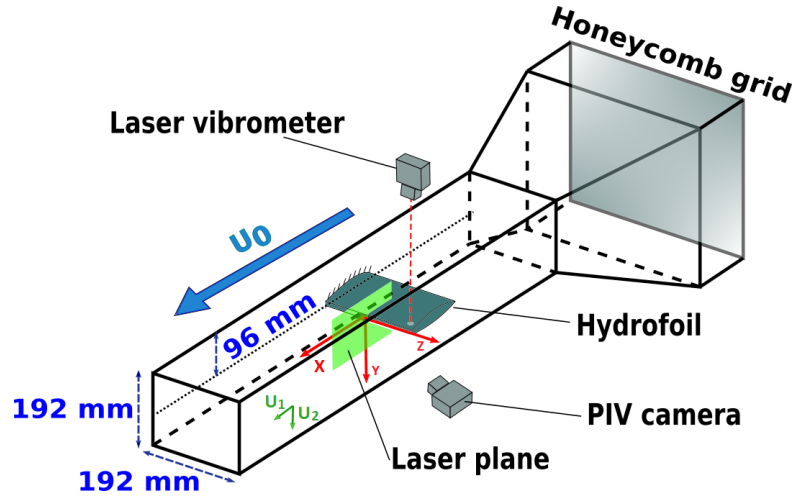


FIGURE 1 – Clamped-free hydrofoil model in the IRENav hydrodynamics test section (Watine, 2023)

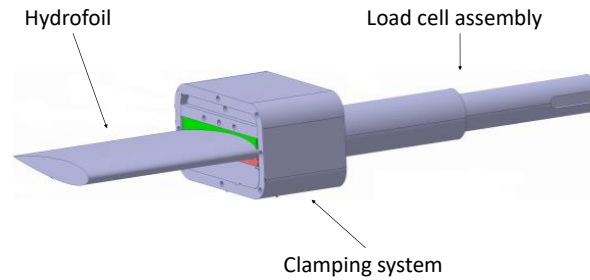


FIGURE 2 – Sketch of the hydrofoil mounting system

In order to mitigate trailing edge vibrations and the associated tonal noise emission, a solution commonly used in naval application is to truncate the hydrofoil trailing edge. A "Truncated" hydrofoil (at 95% of the chord so a trailing edge thickness of  $2 \times 10^{-3}m$ ) of same material and geometry was tested along with

a so called "Tripped" solution for which the turbulence at the pressure side was artificially triggered at mid-chord using a roughness strip of  $0.01m$  width (10% of the chord), manufactured on purpose by using a self-adhesive strip of  $175 \times 10^{-6}m$  thickness, roughened with sandpaper. The resulting mean roughness measured with a roughness meter, was  $4 \times 10^{-6}m$ . Note that the overall roughness height is dominated by the thickness of the strip and is thus close to the displacement value of a laminar boundary layer with no pressure gradient (Blasius solution) at mid chord,  $\delta^* = 1.72 \sqrt{\frac{\nu c}{2U_\infty}} \approx 172.10^{-6}m$  for  $U = 5m/s$ .

### 2.1. Hydrodynamic forces measurements

Hydrodynamic force measurements were performed with the profile fixed on a clamped mounting system (see Figure 2) which increases the foil embedding to ensure maximum vibration results quality. The whole system is assembled in a two axis hydrodynamic balance allowing to measure instantaneous lift, drag and pitching moment about the quarter chord. Only time average values are presented hereafter. For angles of attack ranging from  $0$  up to  $9^\circ$ , set with an accuracy less than  $0.2^\circ$ , steady lift, drag and pitching moment ensue from the average of 10s of the force sensor signals, acquired at a sampling frequency of 1024 Hz. Dimensionless pressure center location is also deduced as  $1/4 - C_m/C_l$  where  $C_m$  is the pitching moment coefficient about the quarter chord point. For reliability, measurements were performed two times and each time with an increasing and decreasing angle of incidence. The steady force and moment precision is less than 2%.

### 2.2. Vibrations and eigenmodes

A PSV-400 Doppler Laser Vibrometer (DLV) that operates thanks to a Doppler-effect with a  $0.02 \mu m s^{-1}$  minimum precision was used to assess the hydrofoil

vibrations. Note that the sensor was disassociated from the tunnel structure in order to limit the impact of pump vibrations.

The hydrofoil eigenmodes, which are identical for the reference and tripped configurations, were determined in still water using a scanning mode technique and exciting the model at the embedding with a custom made vibrating pot at a frequency of 1 Hz. Fifty five points and a reference were used to mesh the profile and to determine the phase in order to reconstruct the deformation. To ensure reliability and to avoid spectral overlap, all vibrations spectrums were calculated with Fast Fourier Transform on an average of 16 data samples of 1s at a frequency acquisition of 9.6 kHz.

Eigenmodes' spatial deformation are featured in Table 1. The first one, close to 50Hz, is associated to the first bending mode. Its frequency is slightly reduced (37Hz) for the truncated model. The second mode, close to 288Hz, can be associated to a second bending mode for which we can see the impact of the non ideal clamping (i.e non zero values at the embedding), due to the intrinsic flexibility of the load cell on which the hydrofoil model is clamped. The associated frequency is also slightly reduced (275Hz) for the truncated model. Another mode between eigenmode 1 and 2, identical for both configuration, was also noticeable in the response spectrums, at a frequency close to 197Hz. It is associated to a rigid mode (not reported in Table 1) for which the flexibility is located on the load cell on which the hydrofoil model is clamped. Mode 3, at 506Hz, is close to a first torsion mode. The associated frequency slightly increases (520Hz) for the truncated configuration. The last mode pointed-out in Table 1 is called Mode 4. It is close to 830Hz for the reference configuration and to 856Hz for the truncated one. It is the one exhibiting the higher amplitude of vibration in the Reynolds number range

explored in the present study. This mode has an area of high deformation close to the trailing edge with a maximum amplitude at mid-span. This eigenmode, labeled "Mode 4", is then called a flapping trailing edge mode.

In order to characterize the hydroelastic trailing edge vibrations of the three hydrofoil models versus the flow velocity (i.e the Reynolds number), measurements were performed using the laser vibrometer focussed on a single point (black dot in Table 1) located at 70% of the chord and 64% of the span. A reflected 3M® S80 patch film was used on the profile to increase the signal quality. As shown in Table 1 the location of the laser vibrometer measurement point does not match the location of maximum deformation of the modes shapes. Amplification coefficients of 1.1 (Mode 1), 2 (Mode 2), 2.1 (Mode 3) and 2.3 (Mode 4) can be used to assess the maximum vibration amplitude located at the tip (Mode 1 and 2), at the tip trailing edge corner (Mode 3) and at the trailing-edge mid-span (Mode 4). Vibration results reported in section 3 are presented in decibels (dB), defined as  $20 \log_{10}(V/V_{ref})$ , where  $V$  is the velocity measured at the black single point (see Table 1) and  $V_{ref} = 0.05m/s$ . Note that for each lock-in range with a specific hydrofoil eigenmode a maximum deformation can be computed from the velocity corrected by the amplification coefficient and divided by the eigenmode frequency. For exemple 0dB, i.e. 0.05m/s, corresponds to a maximum deformation of  $1.1 \times 10^{-3}m$  at the tip (Mode 1),  $3.5 \times 10^{-4}m$  at the tip (Mode 2),  $2.1 \times 10^{-4}m$  at the tip trailing edge corner (Mode 3) and of  $1.4 \times 10^{-4}m$  at the trailing-edge mid-span (Mode 4).

### 2.3. Particle Image Velocimetry analysis

In order to scrutinize the hydrodynamic excitation mechanism, Time Resolved Particle Image Velocimetry (TR-PIV) was carried out with a Nd-Yag double cavity

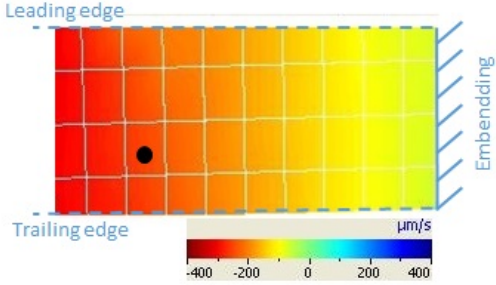
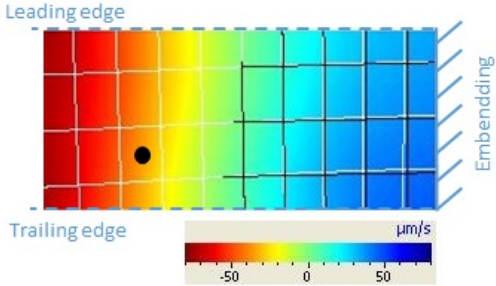
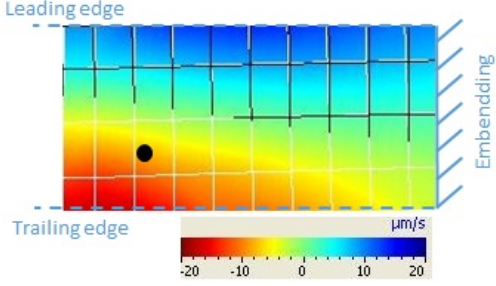
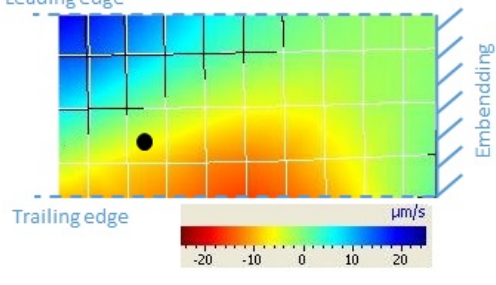
Mode	Reference	Truncated	Modal shape
1	50 Hz	37 Hz	
2	288 Hz	275 Hz	
3	506 Hz	520 Hz	
4	830 Hz	856 Hz	

TABLE 1 – Frequency and mode shape associated to the eigenmodes of reference and truncated configuration : Top view of the hydrofoil, the clamped side of the model is at the right, the leading edge at the top. Black dot corresponds to the point where vibration measurements were performed.

Laser and a SpeedSense 2640 Phantom camera allowing to record 1024x400 pixel frames at 10 000Hz. Post processing with DynamicStudio® adaptative PIV software from Polytech® was performed with an interrogation area of 8x8 pixel and 4 pixel recovery giving rise to 252x99 vectors fields of physical dimensions  $0.054m \times 0.021m$  with spatial resolution of  $0.00021m$ . For each acquisition, 2000 pictures were collected over a period of 0.2s.

In this paper TR-PIV was mainly used to track the pressure side boundary layer transition location. Although the resolution of the velocity field is close to the boundary layer thickness a signature of the boundary layer transition process, which is known to exhibit low frequency modulations and/or intermittent mechanisms, was seen on the histogram of the horizontal velocity measured close to the pressure side. Histogram speed distributions are reported in Figure 3 for two points located on the pressure side of the hydrofoil model, for  $\alpha = 3^\circ$  and  $Re = 8 \times 10^5$ . The point at 97% of the chord exhibits an unimodal distribution, centered at the mean velocity, with a small negative skew, while the point slightly upstream at 83% of the chord shows a multimodal distribution with a small normal distribution centered at a velocity speed close to 40% of the mean velocity. The former, i.e. the unimodal distribution, is the signature of a fully turbulent boundary layer while the later, i.e. the bimodal distribution, is attributed to a transition process for which low frequency modulations and intermittent mechanisms could be responsible for the distribution centered at a velocity speed close to 40% of the mean velocity. An occurrence method with a threshold of 40% was then used to map the transition process area along the pressure side of the hydrofoil. For each vector of the vector field the number for which the horizontal velocity is below 40% of the local mean velocity is divided by the total number of pictures collected (2000). It is then

possible to reconstitute a map where the number of occurrences of low speed is displayed. Results are reported in Figure 3 showing an area in red, between 70 to 85% of the chord, exhibiting the highest occurrence of horizontal velocity below 40% of the local mean velocity, that is associated to the area of transition of the boundary layer. It could be noticed that this occurrence method is more qualitative than quantitative, as no clear transition point location can be identified. Changing the threshold value from 30% up to 50% did not lead to more quantitative results.

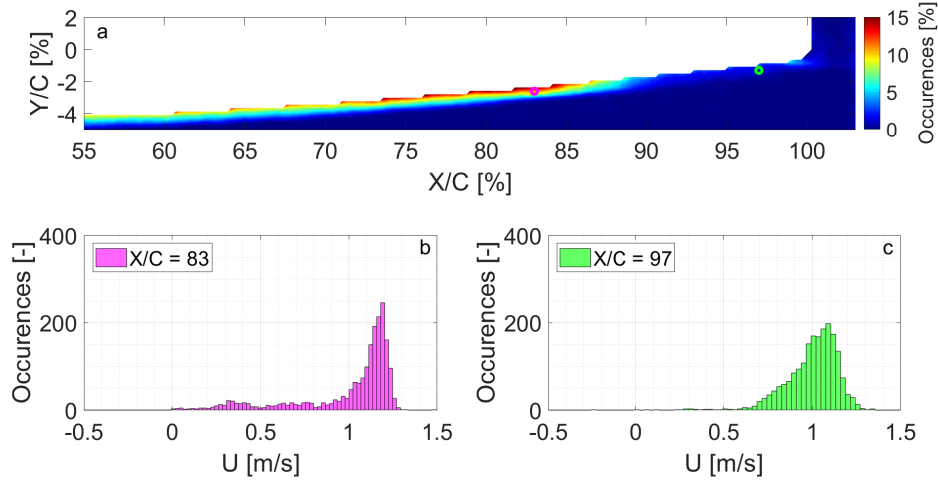


FIGURE 3 – (a) Colormap of the horizontal velocity occurrence (below 40% of the mean horizontal velocity at each point) on the pressure side of the hydrofoil model for  $\alpha = 3^\circ$  and  $Re = 8 \times 10^5$ ; (b & c) Histogram of the horizontal speed distribution at point 1 (83% of the chord) and point 2 (97% of the chord)

Dynamic Mode Decomposition (DMD) was also performed thanks to Fernando Zigunov (2022) [DMD] - Wrapper algorithm in order to identify wake coherent structure. Schmid (2010) showed that DMD method allows to extract dynamic information from experimental flow and can be used to describe the physical mechanisms. DMD reconstruction illustrated in section 3 is a spatial TR-PIV

flow speed vector associated with the frequency exhibiting the highest spatial consistency.

### 3. Results and discussions

#### 3.1. Vibratory response

Hydrofoil vibratory responses were measured for Reynolds numbers  $Re$ , ranging from  $2 \times 10^5$  up to  $12 \times 10^5$  and various angles of attack (AoA), from 0 up to  $10^\circ$ . Vibration response spectrums are presented in Figure 4 for a fixed root angle of attack of  $5^\circ$  as a function of the Reynolds number.

Increasing the velocity, i.e. the Reynolds number, it appears that eigenmodes of the hydrofoil are successively locked. The first one can be observed for  $2 \times 10^5 \leq Re \leq 3.5 \times 10^5$ , at lock-in with a  $190Hz$  structural mode that is, as discussed in 2.2, an experimental artefact (a rigid mode due to non ideal clamping of the hydrofoil).

The second significant lock-in area is observed for  $3.5 \times 10^5 \leq Re \leq 4.7 \times 10^5$ , at lock-in with Mode 2 at a frequency slightly over  $288Hz$ , the natural frequency of Mode 2 measured in still water, see Table 1. The most important lock-in area occurs for  $Re$  ranging from  $6 \times 10^5$  up to  $9 \times 10^5$ , at lock-in with the trailing-edge structural mode 4 for which the natural frequency, in still water, is close to  $830 Hz$ . This flow-induced vibration area is also the one for which the amplitude of vibration are the highest and strong tonal noise emission are observed. Slight frequency shifts with flow speed can also be noticed in this lock-in range.

Besides the three lock-in areas that have been discussed, Figure 4 shows that the first bending mode of the hydrofoil (at frequency close to  $50Hz$ , see Table 1) also vibrates with amplitude increasing with the flow velocity. This can be attributed to a turbulence-induced vibration response due to the residual turbulence of the



incoming flow generating unsteady random hydrodynamic loading and a so-called buffeting response.

One can also note that the first torsion mode of the hydrofoil (mode 3 at frequency close to  $506\text{Hz}$ , see Table 1) is not present in the vibratory response spectrums, suggesting that the modal shape is an important parameter.

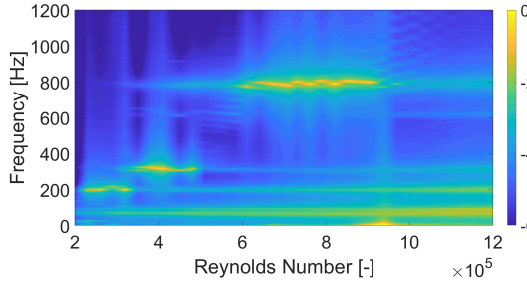


FIGURE 4 – Vibration response spectrum as a function of the Reynolds number for an angle of attack of  $5^\circ$

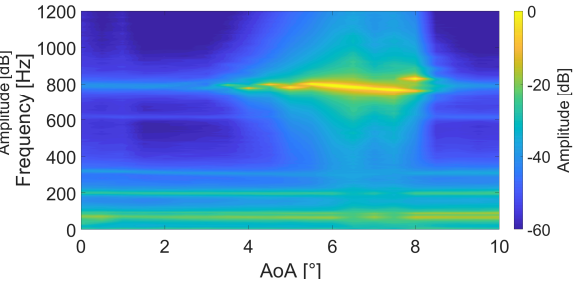


FIGURE 5 – Vibration response spectrum as a function of the angle of attack for  $Re = 8 \times 10^5$

Vibration response spectrums of the hydrofoil at a Reynolds number of  $8 \times 10^5$  are presented in Figure 5 as a function of the angle of attack. Results show that trailing edge vibrations lock-in can only be observed for a specific range of angle of attack  $4 \leq \alpha \leq 8.5^\circ$ . A frequency shift can also be observed. In particular, the coupling frequency slightly decreases with the angle of attack between  $6^\circ$  and  $8.5^\circ$ . One can also note that the observed frequencies at lock-in are close to  $800\text{Hz}$  and thus slightly lower than the one measured for mode 4 in still water ( $830\text{Hz}$ ). Motion-induced hydrodynamic forces should be responsible for that.

Amplitude of the dominant peak in the response spectrums are reported in Figure 6 as a function of the Reynolds number for angles of attack  $5^\circ$ ,  $6^\circ$ ,  $7^\circ$  and  $8^\circ$  that are concerned by trailing edge vibrations according to Figure 5.

For  $\alpha = 5^\circ$  the lock-in is observed for  $5 \times 10^5 < Re < 9 \times 10^5$ . It increases

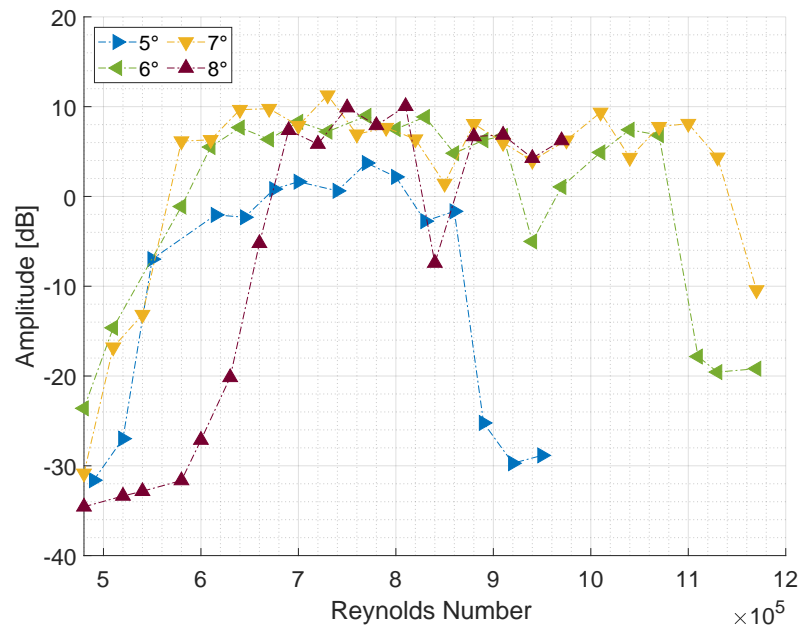


FIGURE 6 – Vibrational dominant peak amplitude as a function of the Reynolds number for several angles of attack

significantly for  $\alpha = 6^\circ$ , starting for  $Re < 5 \times 10^5$  up to  $11 \times 10^5$ , the associated vibration amplitudes are also higher (+6dB). For  $\alpha = 7^\circ$  the trailing edge vibration seems to be slightly strengthened with a lock-out occurring for  $Re$  close to  $12 \times 10^5$ . For  $\alpha = 8^\circ$  the lock-in is significantly delayed, it occurs for  $Re > 6 \times 10^5$ . The associated frequency is also shifted to a higher value (see Figure 6). Unfortunately, measurements could not be performed for  $Re > 10^6$  due to device limitations.

Such vibrations of significant amplitude in a limited range of velocity, associated with a lock-in of the frequency, is typical of Vortex-Induced Vibrations (VIV). VIV mainly concerns structure in cross flow that exhibits a Karman vortex wake organisation, as those with circular or low aspect ratio cross section.

Thanks to TR-PIV and Dynamics Mode Decomposition, a coherent structure in space and frequency has been highlighted in the wake of the hydrofoil (Figure 7) for  $Re = 8 \times 10^5$  and  $\alpha = 5^\circ$ , where trailing edge vibration of significant amplitude was observed (see. Figures 5 and 6). This flow organisation occurs at the same frequency and appears as a vortex street increasing up to 120% of the chord before decreasing in intensity.

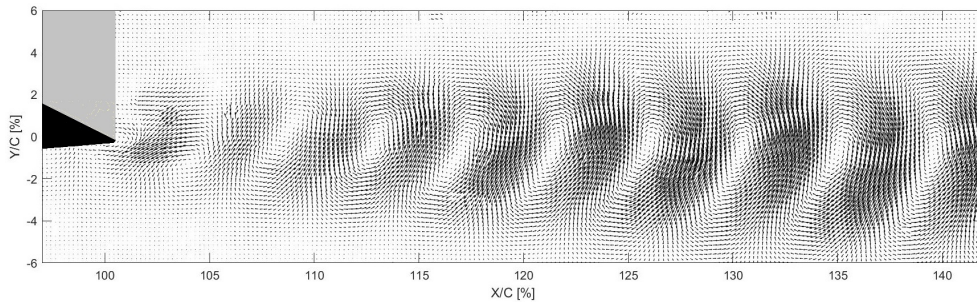


FIGURE 7 – DMD mode shape of the wake at frequency of 783 Hz for  $Re = 8 \times 10^5$  and  $AoA=5^\circ$

Outside the lock-in range no clear vortex organisation can be extracted using the Dynamics Mode Decomposition technique. This indicates that rather than a

Karman vortex wake organisation, the wake signature observed at lock-in is the consequence of a hydroelastic coupling between the trailing edge structural mode of the hydrofoil and a hydrodynamic excitation mechanism occurring close to the trailing edge.

Vibration response spectrums allow us to track a velocity dependent frequency that could be associated to a hydrodynamic excitation mechanism (peak on the response spectrum that does not correspond to a structural mode). Results are reported for various angles of attack in Figure 8 along with the frequency evolution law of Paterson *et al.* (1973) using Equation 1).

Regarding the experimental results one can clearly notice a hydrodynamic excitation mechanism with frequency gradually increasing with the velocity.

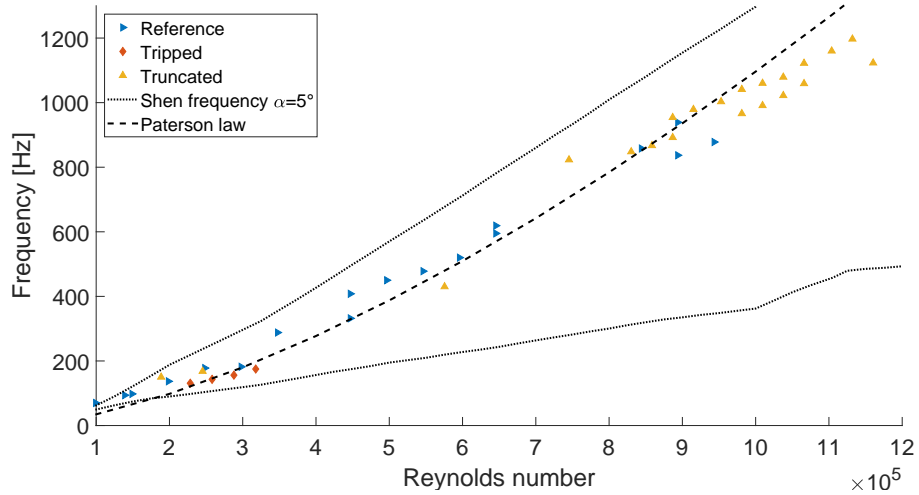


FIGURE 8 – Comparison between experimental frequencies, Shen (1954) stability curve at  $\alpha = 5^\circ$  and Paterson *et al.* (1973) law

It is interesting to notice that the Strouhal law of Paterson *et al.* (1973) is consistent with those results, suggesting that a constant Strouhal number law with reference dimension calculated from the laminar boundary layer thickness of a flat

plate with no pressure gradient could be used.

Flow instability involving Tollmien-Schlichting (TS) waves is known to occur in the boundary layer transition process (Lin , 1945 and Shen, 1954). Here, following the work of Tam (1974), the neutral stability curve of Shen (1954) have been used to calculate the bound frequencies for which Tollmien-Schilting (TS) waves can be amplified during the transition process. Results are reported in Figure 8 for  $\alpha = 5^\circ$ , where bound frequencies have been determined for Reynolds numbers ranging from  $10^5$  up to  $12 \times 10^5$  using pressure side displacement thickness computed at the trailing edge, calculation of a Reynolds number based on the displacement thickness and identification of two bound frequencies using the neutral stability curve of Shen. Pressure side displacement thicknesses at the trailing edge have been computed with the boundary layer solver of XFoil (Drela, 1989). Results reported in Figure 8 show that the observed hydrodynamics signature out of lock-in are included in the frequency domain of amplification disturbance predicted by the neutral stability curve of Shen (1954), suggesting that a pressure side boundary layer transition process occurring close to the trailing edge could be involved.

### 3.2. *Transition point*

In the range of Reynolds numbers for which trailing edge vibration are observed, the transition between a laminar and turbulent boundary layer (BL) occurs before the mid-chord on the suction side. It was verified by XFOIL analysis. Using TR-PIV measurements and the occurrence method presented in section 2.3, boundary layer transition area was tracked on the hydrofoil pressure side for different angles of attack. Results are reported in Figure 9 to 14 for a  $Re = 8 \times 10^5$ . It shows that an area of low speed occurrences, associated to a BL transition area, moves forward to the trailing edge when increasing the angle of attack. Below

to  $5^\circ$  (Figure 9 and 10) the instability area is contained before the trailing edge whereas for  $5^\circ$  (Figure 11) the end of the transition area match the trailing edge point. This could explain why this angle of attack is the one for which the trailing edge vibrations first occurs (see Figure 6).

Between  $6^\circ$  and  $8^\circ$  (Figure 12, 13 and 14) the transition area remains close to the trailing edge while for  $8^\circ$  (Figure 14) the low speed occurrences area is delayed in the wake. Note that the hydroelastic coupling involving trailing edge vibration vanishes for  $\alpha > 8.5^\circ$ .

The location of the transition point close to the trailing edge seems then to be an important condition for trailing edge hydroelastic coupling. An increase in the Reynolds number is known to move the transition point towards the leading edge, which can generate lock-off.

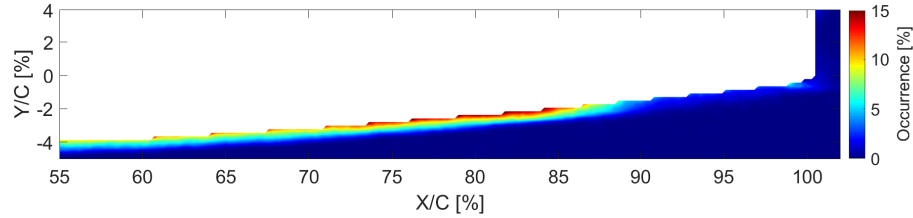


FIGURE 9 – Occurrence method for a Reynolds number of  $8 \times 10^5$  and  $\alpha = 3^\circ$  at pressure side

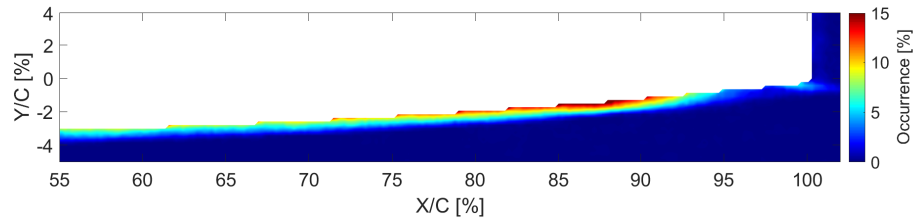


FIGURE 10 – Occurrence method for a Reynolds number of  $8 \times 10^5$  and  $\alpha = 4^\circ$  at pressure side

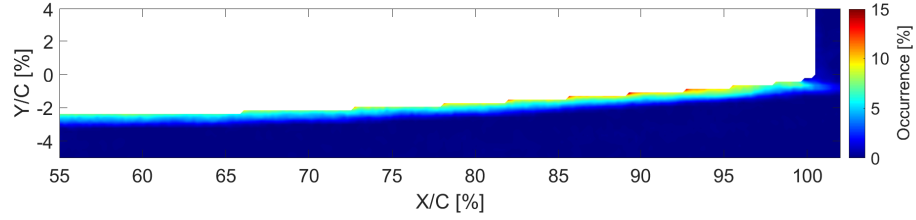


FIGURE 11 – Occurrence method for a Reynolds number of  $8 \times 10^5$  and  $\alpha = 5^\circ$  at pressure side

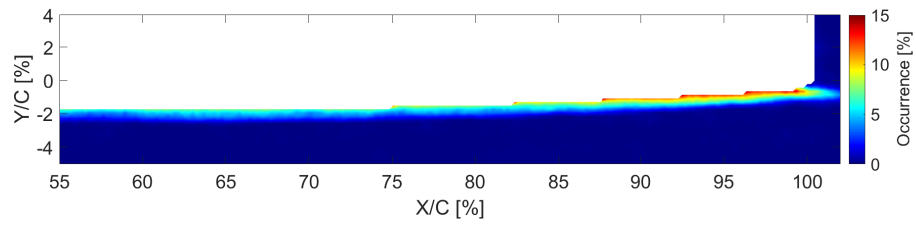


FIGURE 12 – Occurrence method for a Reynolds number of  $8 \times 10^5$  and  $\alpha = 6^\circ$  at pressure side

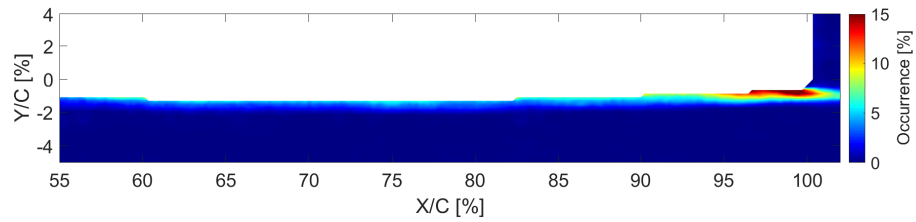


FIGURE 13 – Occurrence method for a Reynolds number of  $8 \times 10^5$  and  $\alpha = 7^\circ$  at pressure side

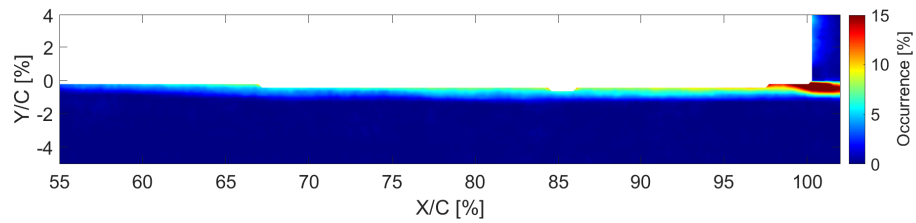


FIGURE 14 – Occurrence method for a Reynolds number of  $8 \times 10^5$  and  $\alpha = 8^\circ$  at pressure side

### 3.3. Control solutions

Amplitude and frequency of the dominant peak in the response spectrums are reported in Figure 15 as a function of the Reynolds number for the "Reference", "Tripped" and "Truncated" configurations, set at an angle of attack of  $5^\circ$ . As for the reference configuration the truncated hydrofoil mode 1 (first bending mode)", the artifact mode at  $190\text{Hz}$ , the mode 2 (second bending) and the mode 4 (flapping trailing edge mode) are successively locked as the Reynolds number increases. Major impact concerns the lock-in with mode 2 and 4. Lock-in with mode 2 is slightly delayed for the truncated hydrofoil but is extended up to  $Re \approx 6 \times 10^5$  in comparison with the reference configuration for which the lock-out occurs for  $Re \approx 5 \times 10^5$ . The lock-in with mode 4 is also significantly delayed for the truncated hydrofoil, it occurs for  $Re \approx 7.3 \times 10^5$  in comparison with the reference configuration for which the lock-in starts for  $Re \approx 6.1 \times 10^5$ . This can not be simply explained by the increase of 3% of the mode 4 natural frequency for the truncated hydrofoil. As the lock-out is slightly delayed for the truncated configuration the range of lock-in is then significantly reduced but the amplitude reported in Figure 15 shows an increase up to 5 dB.

In comparison the tripped configuration is very effective to suppress the lock-in with mode 2 and 4 but significantly increase the fluid-elastic coupling with the first bending mode. Vibration of significant amplitude are now observed for  $1 \times 10^5 \leq Re \leq 2.5 \times 10^5$ . A slight resonance with both the artifact mode at  $190\text{Hz}$  and mode 2 still remains prior to a turbulence-induced vibration response, with amplitude gradually increasing with the velocity, involving the first bending mode for which the natural frequency is close to  $50\text{Hz}$ . PIV images of the pressure side between 55% and 100% of the chord have been recorded in the tripped configu-



ration. No low speed occurrence was detected, which suggest that the boundary layer transition was located before 55% of the chord and thus immediately after the rough strip.

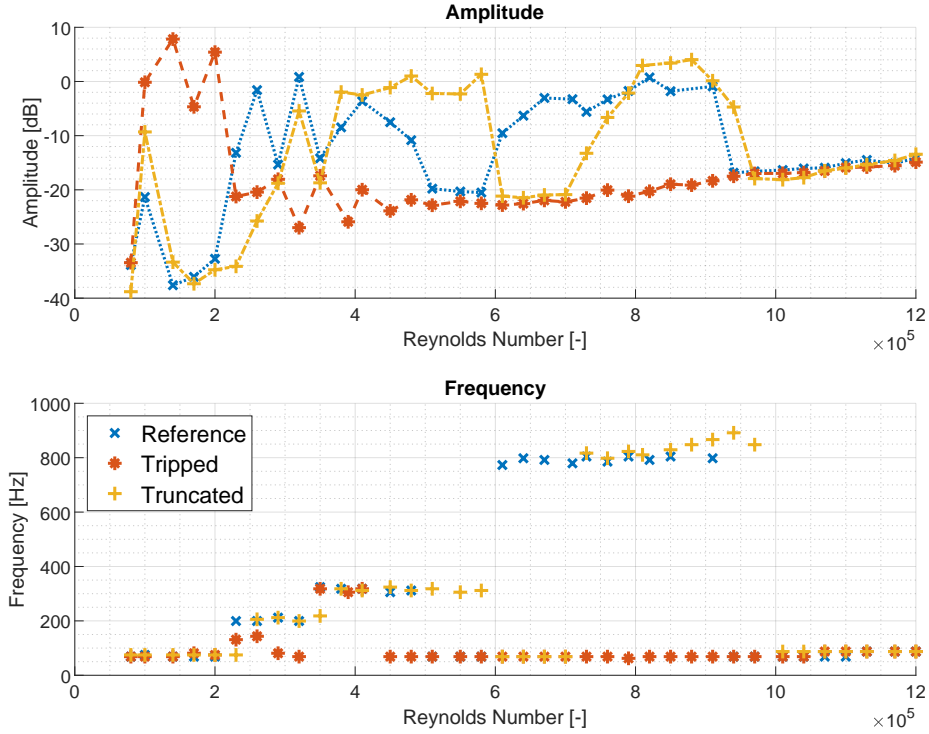


FIGURE 15 – Vibrational dominant peak amplitude and frequency for the three cases in function of Reynolds number and for  $AoA=5^\circ$

Both the truncated and tripped configurations have also been compared with the reference hydrofoil in term of hydrodynamic performances. Lift-to-drag ratio as a function of the angle of attack is presented in Figure 16 for a Reynolds number of  $8 \times 10^5$ . Loss of performance regarding the reference configuration,  $[C_l/C_d]/[C_l/C_d]_{ref} - 1$  (expressed in percent) is also reported in this Figure. Note that hydrodynamic forces measurements were not allowed beyond  $9^\circ$  to preserve

the integrity of the load sensor.

The truncated configuration has a strong impact on the lift-to-drag ratio with a loss close to 10% in the range of angles of attack for which the lift-to-drag ratio is the highest (close to  $6^\circ$ ). The loss in performances is much lower for tripped solution method, with a loss close to 4% for angles of attack close to  $6^\circ$ . Moreover, the tripped configuration doesn't affect the lift-to-drag ratio performance for small angles of attack in comparison with the truncated configuration for which the loss of performance for  $\alpha = 1^\circ$  is close to 20%.

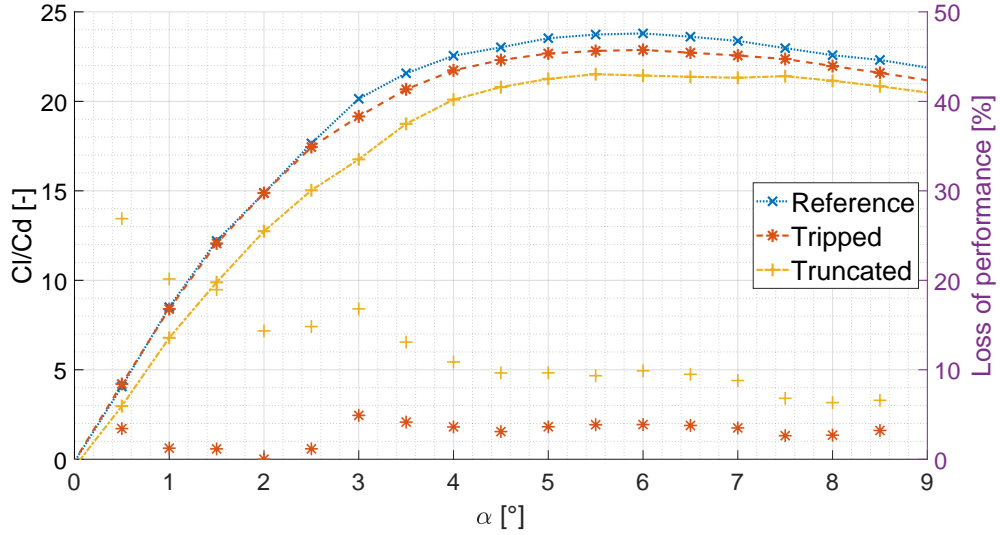


FIGURE 16 – Lift-drag ratio for the three configurations in function of angle of attack for  $Re=8 \times 10^5$

Evolution of both the pitching moment coefficient and pressure center location, as a function of the angle of attack, are reported in Figure 17 for the three configurations and  $Re = 8 \times 10^5$ . A peculiar behaviour can be observed for the reference configuration. A bump on the moment coefficient appears for angles of attack concerned with trailing edge vibrations. In Figure 17, the bump starts close

to  $6^\circ$  up to  $9^\circ$ . This nose-up behaviour of the pitching moment is associated to a decrease of the pressure centre location that moves down to 23.5% of the chord location for  $\alpha = 8^\circ$  for which the tonal emission is the highest. The truncated configuration softens the bump on the moment coefficient, with a maximum nose-up effect located at lower angle of attack, close to  $7^\circ$ , while for the tripped configuration the bump is fully suppressed. An overall increase of the pitching moment coefficient can however be noticed for both truncated and tripped configurations. As a consequence the pressure center location is shifted toward the leading-edge. For  $\alpha = 2^\circ$  it is located at 23.6% of the chord for both the truncated and tripped configurations while it is located up to 24.3% for the reference configuration. It then linearly goes toward the mid-chord with the angle of attack increasing.

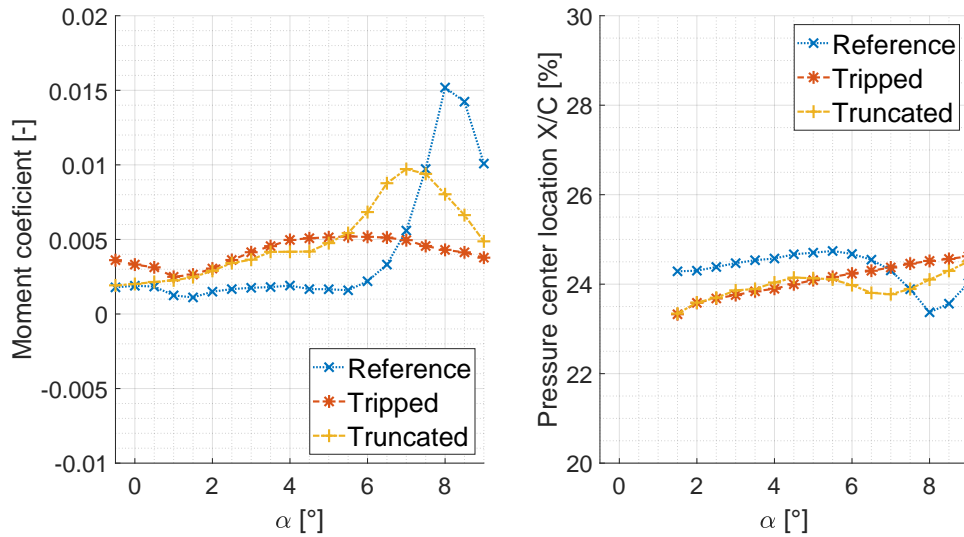


FIGURE 17 – Pitching moment coefficient about the quarter chord and pressure centre location as a function of the angle of attack for the reference, tripped and truncated configurations ;  $Re=8 \times 10^5$

#### 4. Discussion

Results reported in the present study suggest that trailing edge vibrations of hydrofoil and the associated tonal noise emission are the consequence of hydro-elastic coupling mechanisms occurring in a limited range of velocity (i.e. Reynolds number) and for a limited range of angles of attack. Three conditions have to be satisfied to observe such mechanism. First, the hydrofoil needs to operate at critical Reynolds number  $Re \sim 10^5$ , meaning that either the suction or the pressure side needs to be partially laminar. Second, the location of the pressure side boundary layer transition needs to be close to the trailing edge that is an area of maximum amplification of perturbation due to the trailing mode shape (see mode 4 in Table 1). And third, the hydrofoil natural frequency in still water needs to be in the bounded frequency of amplification of the unstable fluid mode, i.e. the Tollmien–Schlichting (TS) waves.

With the NACA0015 hydrofoil used in the present study, hydroelastic trailing edge vibrations of significance amplitude were observed at moderate angles of attack  $4 \leq \alpha \leq 8.5^\circ$  for Reynolds number  $5.5 \times 10^5 < Re < 11.5 \times 10^5$  for which the pressure side boundary layer transition is located close to the trailing edge with a range of frequency amplification of the TS wave allowing a lock-in with the hydrofoil trailing edge structural mode. Note that for this specific range of Reynolds numbers the suction side was almost fully turbulent. In this hydroelastic coupling configuration tonal noise can be observed along with coherent vortex wake organisation.

This is consistent with the work of Nakano *et al.* (2007), that pointed out a strong dependence of the angle of attack on tonal noise emission. It is also in accordance with the work of Probsting *et al.* (2015), showing that transition at

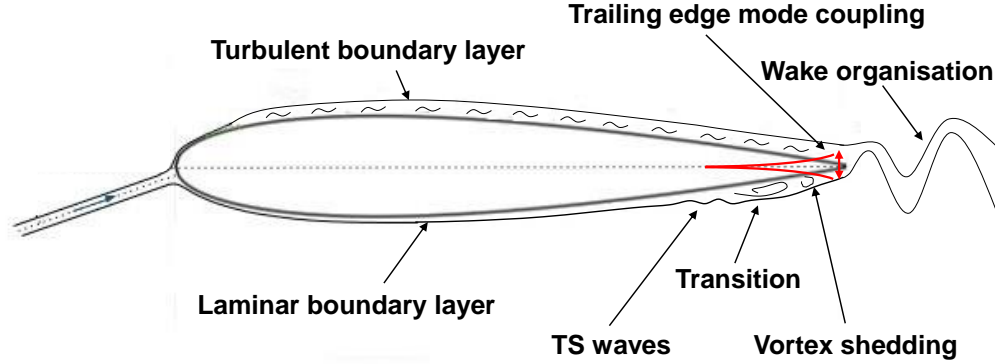


FIGURE 18 – Schematization of hydrodynamics phenomena and trailing edge hydroelastic coupling

the suction side impacts tonal noise emission when it's sufficiently close to the trailing edge. The three conditions leading to trailing edge vibrations and tonal noise emission can also be reached for transition mechanisms involving laminar separation bubble (LSB). Marxen *et al.* (2003) showed that transition in a separation bubble can be driven by convective primary amplification of Tollmien-Schlichting waves, resulting in spanwise rollers that are shed from the separation bubbles. This was also highlighted by Ducoin *et al.* (2019), who pointed out a coherent vortex shedding organisation downstream the LSB, further degenerating in turbulence after the breaking of T-S waves.

## 5. Conclusion

Trailing-edge vibrations on a NACA0015 clamped hydrofoil were investigated experimentally. An hydrodynamic excitation mechanism was also questioned based on unsteady flow analysis, boundary layer transition consideration and previous studies conducted on airfoils. Hydroelastic trailing edge vibrations of significance amplitude were observed at moderate angles of attack  $4 \leq \alpha \leq 8.5^\circ$  and in a

limited range of Reynolds number  $5.5 \times 10^5 < Re < 11.5 \times 10^5$  for which the pressure side boundary layer transition is located close to the trailing edge, with a frequency signature allowing a lock-in with the hydrofoil trailing edge structural mode. It was shown that the Strouhal law of Paterson *et al.* (1973) is consistent with the frequency evolution of the hydrodynamic excitation mechanism with the flow velocity. It thus can be used to predict the lock-in with structural modes. Using the neutral stability curve of Shen (1954), it was also shown that trailing edge vibration leading to strong tonal noise emission could be the consequence of trailing edge hydroelastic coupling in the bounded frequency of amplification of the unstable fluid mode, i.e. the Tollmien–Schlichting (TS) waves.

In conclusion trailing-edge vibrations on hydrofoil need three conditions : (1) the hydrofoil has to operate at critical Reynolds  $Re \sim 10^5$ , (2) the location of the boundary layer transition needs to be close to the trailing edge that is an area of maximum amplification of perturbation of the structural trailing-edge mode shape and (3) the trailing-edge natural frequency has to be in the bounded frequency of amplification of the Tollmien–Schlichting waves.

Two passive solutions were tested to mitigate this hydroelastic flow-induced vibration : a truncated hydrofoil and a triggered hydrofoil. The truncated hydrofoil slightly mitigate by triggering the pressure side boundary layer transition ahead of the trailing edge. It eliminates the trailing edge vibrations with negligible impact on the hydrofoil hydrodynamics performances.

## Références

H. Arbey, J. Bataille, Noise generated by airfoil profiles placed in a uniform laminar flow, *Journal of Fluid Mechanics*, 134 (1983) 33–47.

- W.K. Blake, Excitation of plates and hydrofoils by trailing edge flows. *Journal of Vibration, Acoustics, Stress, and Reliability in Design*, 106 (1984) 351–363.
- L.T. Clark, The radiation of sound from an airfoil immersed in a laminar flow, *Trans ASME A : Journal of Engineering Power*, 93 (1971) 366–376.
- M. Drela, XFOIL : An analysis and design system for low Reynolds number airfoils, in *Low Reynolds number aerodynamics, Low Reynolds Number Aerodynamics : Proceedings of the Conference Notre Dame, Indiana, USA, 5–7 June 1989* 1–12, Springer, 1989.
- A. Ducoin, J.A. Astolfi, M.L. Gobert, An experimental study of boundary-layer transition induced vibrations on a hydrofoil, *Journal of Fluids and Structures*, 32 (2012) 37–51.
- A. Ducoin, J.A. Astolfi, Wall-pressure fluctuations of laminar separation bubble based on direct numerical simulation and experiments over a hydrofoil at  $Re=450,000$ , *European Journal of Mechanics-B/Fluids*, 76 (2019) 132–144.
- C.C. Lin, On the Stability of Two-Dimensional Parallel Flows, *Quarterly of Applied Mathematics*, 3 (1945) 117–142.
- O. Marxen, M.Lang, U.Rist, S.Wagner, A combined experimental/numerical study of unsteady phenomena in a laminar separation bubble, *Flow, Turbulence and Combustion*, 71 (2003) 133–146.
- A. McAlpine, E.C. Nash, M.V. Lowson, On the generation of discrete frequency tones by the flow around an aerofoil, *Journal of Sound and Vibration*, 5 (1999) 753–779.

- T. Nakano, N. Fujisawa, Y. Oguma, Y. Takagi, S. Lee, Experimental study on flow and noise characteristics of NACA0018 airfoil, *Journal of Wind Engineering and Industrial Aerodynamics*, 7 (2007) 511–431.
- E.C. Nash, M.V. Lowson, A. McAlpine, Boundary-layer instability noise on aerofoils, *Journal of Fluid Mechanics*, 382 (1999) 27–61.
- R.W. Paterson, W. Robert, P.G. Vogt, M.R. Fink, C.L. Munch, Vortex noise of isolated airfoils, *Journal of Aircraft*, 5 (1973) 296–302.
- S. Pröbsting, S. Yarusevych, Laminar separation bubble development on an airfoil emitting tonal noise, *Journal of Fluid Mechanics*, 780 (2015) 167–191.
- P.J. Schmid, Dynamic mode decomposition of numerical and experimental data, *Journal of fluid mechanics*, 656 (2010) 5–28.
- S.F. Shen, Calculated amplified oscillations in the plane Poiseuille and Blasius flows, *Journal of the aeronautical sciences*, 21 (1954) 62–64.
- C.K.W. Tam, Discrete tones of isolated airfoils, *The Journal of the Acoustical Society of America*, 6 (1974) 1173–1177.
- G.H Toebe, P.S Eagleson, Hydroelastic vibrations of flat plates related to trailing edge geometry, *Journal of Basic Engineering* 83 (1961) 671–678.
- Y. Watine, C. Gabillet, B. Lossouarn, J.F Deü, J.A Astolfi, Vortex-induced vibrations of a cantilevered blunt plate : POD of TR-PIV measurements and structural modal analysis *Journal of Fluids and Structures* 117 (2023) 103832
- F. Zigunov, Dynamic Mode Decomposition [DMD] - Wrapper, MATLAB Central File Exchange, (2021).